KSCE Journal of Civil Engineering (2022) 26(6):2952-2965
DOI 10.1007/s12205-022-1770-1

pISSN 1226-7988, eISSN 1976-3808
www.springer.com/12205

Tunnel Engineering

A Semi-analytical Solution of Face Extrusion Deformation Considering Nonlivnear Changes of Rock Mass Mechanical Parameters

Zhi-long Wang[a], Ming-nian Wang[a], Cheng Lyu[b], and Da-gang Liu[a]

[a]*Key Laboratory of Transportation Tunnel Engineering, Ministry of Education, Southwest Jiaotoug University, Chengdu 610031, China*
[b]*College of Water Resource and Hydropower, Sichuan University, Chengdu 610065, China*

ARTICLE HISTORY

Received 21 October 2021
Revised 20 December 2021
Accepted 5 January 2022
Published Online 15 March 2022

KEYWORDS

Variable confining stress
Circular and non-circular tunnel
Face extrusion deformation
Elastic-plastic solution
M-C failure criterion

ABSTRACT

The stress state of rock mass is redistributed after the tunnel excavation, resulting in different confining stress at different radial distances. Relevant studies demonstrate that the mechanical characteristics of rock are related with the confining stress, causing various the mechanical parameters of rock mass at different radial distances. This paper aims to take these kinds of mechanical properties of rock mass into the analytical solutions of stress and deformation around the tunnel face. Firstly, the calculation formulas of the rock mass mechanical parameters changing with the confining stress is determined based on the existing rock triaxial test data. Then, a new model considering the influence of confining stress is proposed based on Mohr-Coulomb (M-C) failure critical. At the same time, an given radial length increment divides the plastic zone into a series of concentric annuli. The finite difference approach may be used to compute consecutive stress and strain increases for each annulus. A comparative analysis of the Pierpaolo Oreste's model and the proposed model is carried out through calculation examples, and the results show that: ignoring the effect of the confining stress on the mechanical parameters of rock mass, the plastic radius of the tunnel face will be smaller than the actual value, and the face extrusion deformation value will be larger. It is emphasized that the influence of confining stress on the mechanical parameters of rock mass should be considered in actual engineering calculations, especially the high initial stress rock mass. Finally, combined with the numerical calculation model, the rationality of the application of the circular tunnel elastoplastic model in the non-circular tunnel is verified.

1. Introduction

Full-face excavation has been increasingly used in tunnel construction to make tunnel construction more systematic and efficient in different conditions, such as poor quality ground, squeezed, or unstable ground (Giovanni, 2016). The designer not only must evaluate the tunnel wall's "convergence" but also the tunnel face "extrusion" during the preliminary study stage. Experience has shown that the extrusion analysis of the core-face is the most important part of the rock mass's deformation response to ensure the continuous progress (Lunardi, 2008; Cantieni et al., 2011; Giovanni, 2016). According to previous studies, there have been many theoretical calculation methods for calculating the convergence deformation and extrusion deformation.

Previous researchers found that the elastic-plastic solutions of tunnel were typically generated using semi-analytical and analytical approaches based on plane strain assumption. For simplicity, the elastic-perfectly plastic theory was used in these accessible solutions (Brown et al., 1983; Carranza-Torres and Fairhurst, 1999, 2000; Kim, 2006; Sharan, 2003, 2005, 2008; Lee and Pietruszczak, 2008; Park et al., 2008; Wang et al., 2010; Serrano et al., 2011). However, it is commonly observed in the field and laboratory that rock mass with average quality tends to show strain-softening behavior during the post-failure stage (Varas et al., 2005; Cai et al., 2007). Therefore, in recent years, the effort was made by many researchers to account for the strain-softening effect (Alonso's model (Alonso et al., 2010), Lee's model (Lee and Pietruszczak, 2008), Alejano's model (Alejano et al., 2010; Alejano et al., 2012), and Lan Cui's model (Cui et al., 2015)). The critical plastic softening parameter η^* controls the transition from plastic softening to the residual stage, which is essential for a reasonable solution because it affects the

CORRESPONDENCE Cheng Lyu lvchengaust@163.com College of Water Resource and Hydropower, Sichuan University, Chengdu 610065, China

ⓒ 2022 Korean Society of Civil Engineers

mechanical parameters of rock mass. As a result, the determination of η^* in theoretical calculations is extremely important for strain-softening materials. Among them, the Alonso's model, Lee's model, and Alejano's model regarded η^* as constant. However, laboratory measurements show that the confining stress has a significant impact on rock mass mechanical characteristics such as η^*, shear strength, and dilatancy, and the point is that the η^* changes with the confining stress. That is to say that the η^* is not constant in the plastic zone. Therefore, Lan Cui's model is proposed considering the influence of confining stress in the derivation of elastoplastic analytical solution.

The calculation model for extrusion deformation of the tunnel face has also made great progress. The stress state ahead of the tunnel face can be approximatively using spherical cavity problems when the tunnel is fully excavated, especially when the lining is installed quite close to the tunnel face. Based on the H-B failure criterion, Carranza-Torres and Fairhurst (Carranza-Torres and Fairhurst, 1999) presented a unified closed-form formulation, and it is applicable to both cylindrical and spherical cavities. Besides, Yu (2000) investigated the spherical cavity expansion problem in Tresca and M-C media. In addition, Wang et al. (2011) have provided analytical formulations in brittle plastic M-C and classic form H-B medium based on the theoretical approach used by Park et al. (Kim, 2006). In the situation of deep tunneling through weak ground Vrakas and Anagnostou (2014) has provided a big strain elastoplastic solution. With the development of rock mechanics theory, an extrusion deformation model of tunnel face considering the strain-softening characteristics is proposed by Tan (Cheng, 2020). However, the Chenghua Tan's model still sets η^* as constant, and also does not consider the influence of confining stress on the critical plastic softening parameter.

Although more in-depth research has been conducted on the strain-softening characteristics of rock mass, it has been proved that the mechanical parameters of rock mass change with the confining stress. However, the calculation formula for characterizing the non-linear characteristics of mechanical parameters of rock mass through the critical plastic softening parameter (such as the calculation formula mentioned in the Lan Cui's model) is more complicated and requires more calculation parameters. At the same time, it does not truly reflect the change characteristics of mechanical parameters with confining pressure. In actual engineering applications, it is inevitable that errors in the calculation results will occur.

Therefore, the object of this paper is to establish the corresponding calculation model between the rock mass mechanical parameters and the confining stress and to create a new numerical procedure considering the influence of confining stress in the analytical solutions. First of all, the changes of rock mass mechanical parameters with confining stress are analyzed based on the triaxial test data. Secondly, the finite difference solution of the stress and deformation of tunnel face in the deep tunnel is derived combining with the characteristics of rock. In addition, the importance of considering the influence of confining stress on the rock mass mechanical parameters in the elastoplastic analysis is further analyzed based on a series of parametric studies. Finally, through the numerical calculation model, the application effect of the proposed model in non-circular caverns is compared and analyzed, and the rationality of its application in non-circular caverns is proved.

2. Problem Description

2.1 Mechanical Properties of Soft Rock

As described in the Introduction, many researchers have proved that the mechanical properties of soft rock (such as deformation and strength characteristics) are closely related to the confining stress, thus the mechanical properties of soft rock under different confining stress are quite different. The phyllite is selected as an example to briefly describe in this work, and the data analyzed in this work comes from R. Gholami · V. Rasouli's work (Gholami and Rasouli, 2014).

2.2 Deformation Parameters

Young's modulus and Poisson's ratio of rock are the two most basic indicators to describe rock deformation characteristics. At the same time, they also control indexes which characterize the rock deformation characteristics in geotechnical engineering calculation and analysis. Therefore, this section focuses on the analysis of the influence of confining stress on the two deformation parameters of Young's modulus and Poisson's ratio, as shown in Figs. 1 and 2. It can be seen that the Young's modulus shows a nonlinear increasing trend with the increase of confining stress (in Fig. 1). That is, the Young's modulus is a function with the confining stress as a variable ($E = a(\sigma_3 + 1)^b$, where a and b are constants). However, Poisson's ratio has no obvious change trend with the increase of confining stress (in Fig. 2).

2.3 Strength Parameters

A large number of rock mechanical tests have proved that the rock failure mode is mainly shear failure. In the calculation and analysis of rock mechanics, it is usually assumed that the failure (yield) strength of the rock is controlled by the shear strength. M-C strength theory was used to analyze the shear strength of rocks in this work. The peak strength of rock under different confining stress conditions is obtained based on the rock triaxial test, as shown in Fig. 3. It can be seen that the rock strength increases with the increase of confining stress, and the growth trend has significant nonlinear characteristics.

At the same time, Mohr circles were drawn under different confining stress in the τ-σ plane, and the Mohr strength envelope was drawn (as shown in Fig. 4). According to the Mohr strength theory, in order to analyze the change law of soft rock shear strength under different confining stress conditions. Furthermore, the tangent of the strength envelope under different confining stress can be obtained (the line AB in Fig. 4) by deriving the Mohr strength envelope. Therefore, the internal friction angle and cohesion under different confining stress conditions are obtained, as shown in Table 1. It can be seen that the internal friction angle decreases

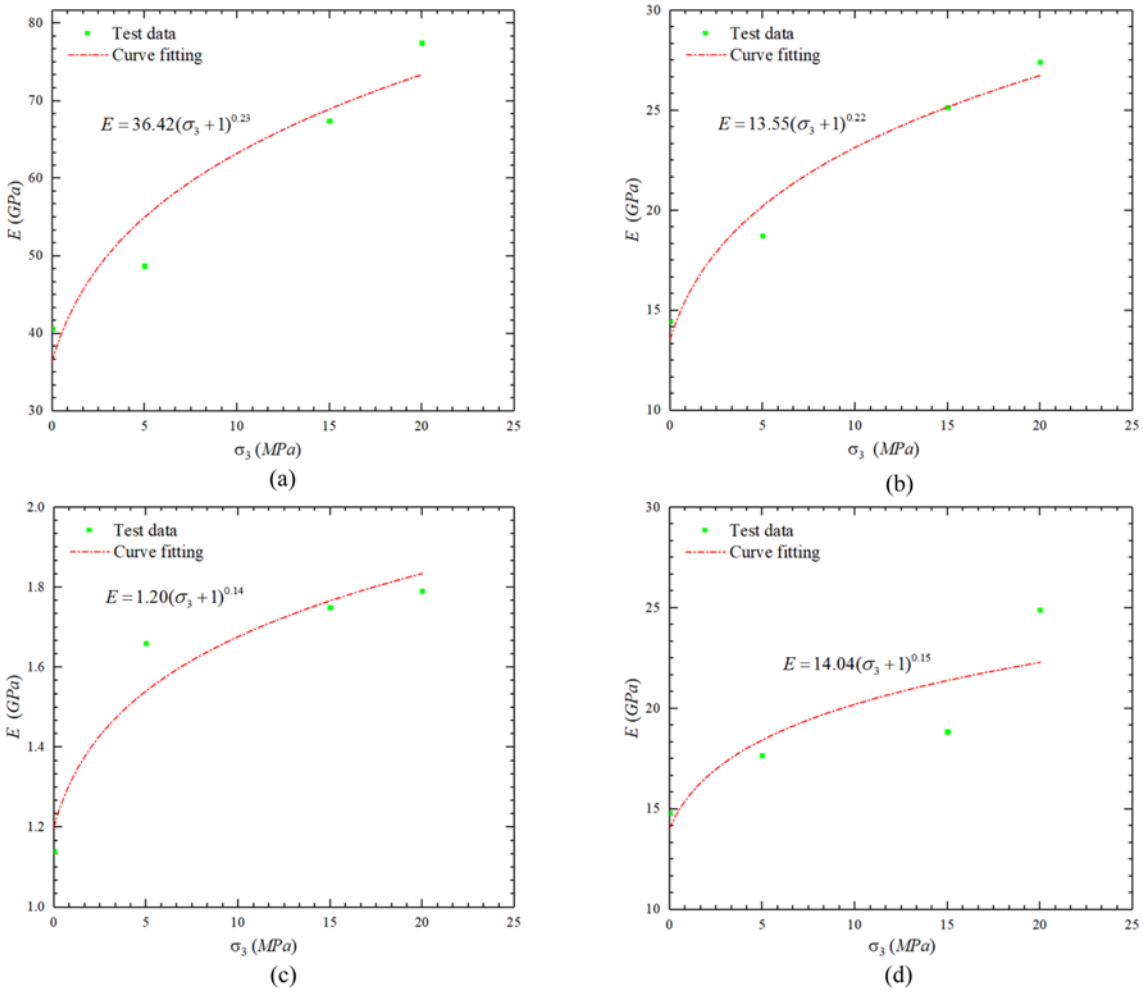

Fig. 1. Variation Curve of Young's Modulus under Different Confining Stress (Gholami and Rasouli, 2014): (a) Carbonaceous Phyllite, (b) Chlorite Phyllite, (c) Sericite Phyllite, (d) Quartz Phyllite

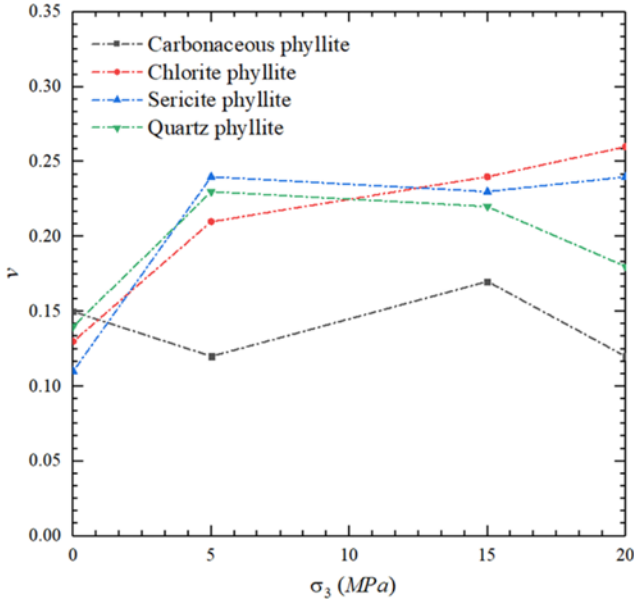

Fig. 2. Variation Curve of Poisson's Ratio under Different Confining Stress (Gholami and Rasouli, 2014)

nonlinearly with the increase of the confining stress and the cohesive increases nonlinearly with the increase of the confining stress. The internal friction angle and cohesion are both functions with the confining stress as a variable as the same as Young's modulus. The expressions of internal friction angle and cohesion are $\varphi = aln(\sigma_3+1)+b$ and $c = a(\sigma_3+1)^b$, respectively.

From the above analysis, it can be seen that the mechanical parameters of rock mass change with the change of confining stress. Therefore, the change of mechanical parameters needs to be considered in the derivation process of the proposed model. It should be noted that although the rock mechanical parameter change model is different under different geological conditions, the expressions will not affect the theoretical derivation process of this paper. In the later application, researchers can replace the corresponding model in the theoretical derivation process of this paper based on related research.

2.4 Basic Model

The behavior of a deep tunnel's tunnel face may be studied using the spherical symmetry hypothesis with a particular approximation,

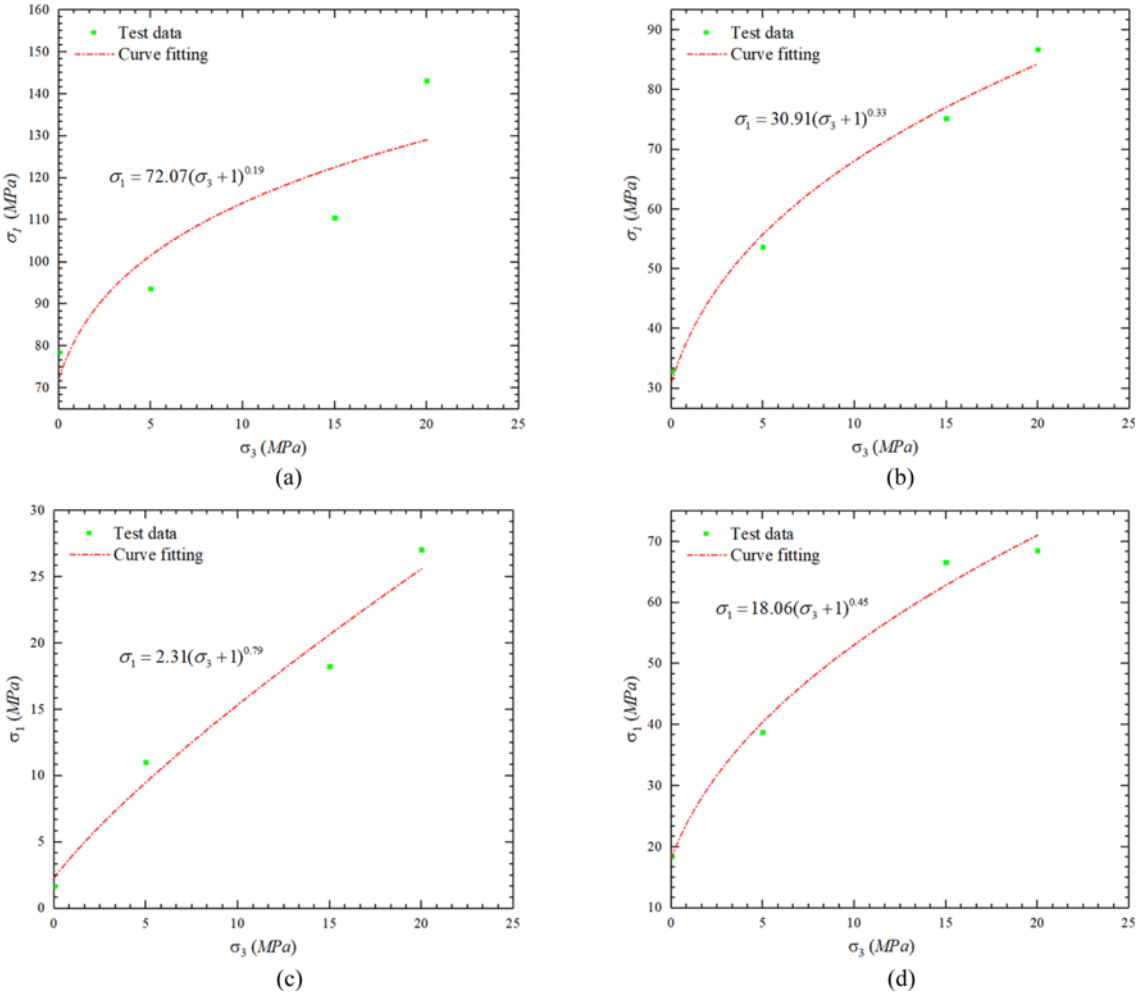

Fig. 3. Variation Curve of Rock Strength under Different Confining Stress (Gholami and Rasouli, 2014): (a) Carbonaceous Phyllite, (b) Chlorite Phyllite, (c) Sericite Phyllite, (d) Quartz Phyllite

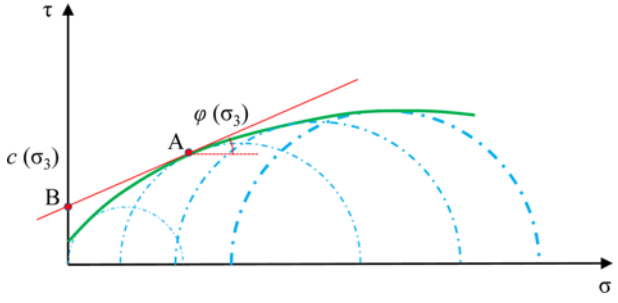

Fig. 4. Mohr Stress Circle and Strength Envelope

which considers a hemispherical void with a radius R_i in a homogeneous and isotropic material initially exposed to a hydrostatic pressure P_0, as shown in Fig. 5. The radial displacements value obtained on the surface of sphere is the estimated value of the average extrusion displacement of tunnel face. For the purpose of simplicity, the stress condition created by tunnel support pressure near the tunnel face is ignored.

2.5 Yield Function

Assuming that the yielding of the rock mass is controlled by the yielding function:

$$f(\sigma_\theta, \sigma_r) = \sigma_\theta - \sigma_r - F(\sigma_r), \tag{1}$$

where σ_ϑ and σ_r are the major and minor principal stresses, respectively.

For M-C rock mass, $F(\sigma_r)$ in Eq. (1) becomes

$$F(\sigma_r) = (N(\sigma_r)-1)\sigma_r + Y(\sigma_r), \tag{2}$$

where $N(\sigma_r)$ and $Y(\sigma_r)$ are the strength parameters defined in terms of friction angle $\varphi(\sigma_r)$ and cohesion $c(\sigma_r)$, as shown in Eqs. (3) and (4):

$$N(\sigma_r) = \frac{1+\sin\varphi(\sigma_r)}{1-\sin\varphi(\sigma_r)}, \tag{3}$$

$$Y(\sigma_r) = \frac{2c(\sigma_r)\cos\varphi(\sigma_r)}{1-\sin\varphi(\sigma_r)}. \tag{4}$$

2.6 Plastic Potential Function

It is assumed that the plastic deformation of rock mass obeys the non-associative flow rule, and the plastic potential function and

Table 1. The Calculation Model of Mechanical Parameter Variable Confining Stress

Lithology	Mechanical parameters	Model	Correlation coefficient
Carbonaceous phyllite	E	$E = 36.42(\sigma_3+1)^{0.23}$	0.87
	c	$c = 70.42(\sigma_3+1)^{0.13}$	0.97
	φ	$\varphi = -11.65ln(\sigma_3+1)+88.12$	0.92
Chlorite phyllite	E	$E = 13.55(\sigma_3+1)^{0.22}$	0.95
	c	$c = 29.28(\sigma_3+1)^{0.22}$	0.96
	φ	$\varphi = -10.17ln(\sigma_3+1)+86.04$	0.94
Sericite phyllite	E	$E = 1.20(\sigma_3+1)^{0.14}$	0.89
	c	$c = 1.87(\sigma_3+1)^{0.39}$	0.92
	φ	$\varphi = -5.67ln(\sigma_3+1)+61.36$	1.00
Quartz phyllite	E	$E = 14.04(\sigma_3+1)^{0.15}$	0.81
	c	$c = 16.45(\sigma_3+1)^{0.29}$	0.96
	φ	$\varphi = -8.49ln(\sigma_3+1)+84.14$	0.96

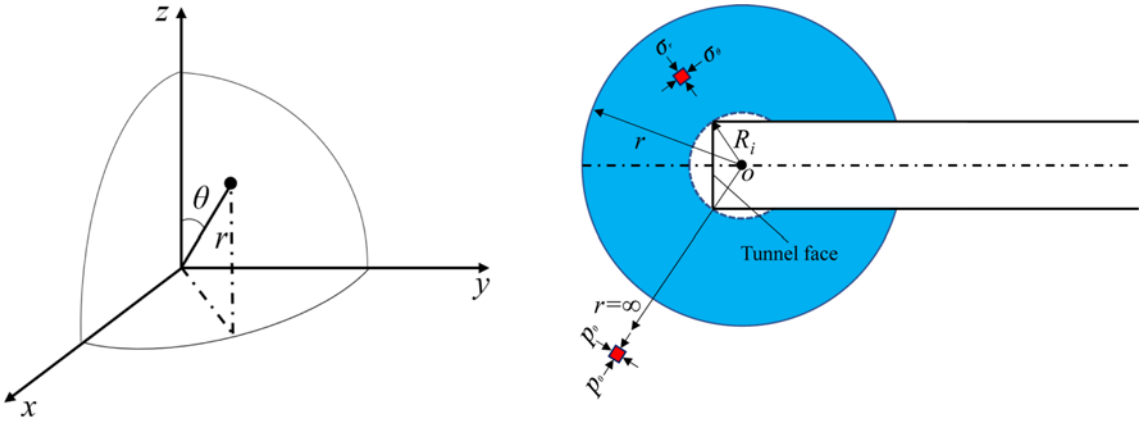

Fig. 5. Schematic Illustration for Tunnel during Full-Face Excavation: (a) Geometry of the Problem of a Spherical Void for the Study of Tunnel Face in the Deep Tunnel, (b) Longitudinal Section of the Tunnel (r: distance of a point from the center of the sphere; x, y, and z: cartesian axes; σ_ϑ: circumferential stress; σ_r: radial stress; R_i: internal radius of the sphere; P_0: lithostatic stress present for $r = \infty$.)

the yield function have the same form. It just replaces the friction angle φ with the dilatancy angle ψ. Thus the plastic potential function based on the M-C yield criterion can be written as

$$g^{M-C}(\sigma_\theta,\sigma_r) = \sigma_\theta - \sigma_r - (N_\psi - 1)\sigma_r - Y_\psi \,. \tag{5}$$

Based on the plastic increment theory, the tangential and radial strains in the plastic zone are as follows:

$$d\varepsilon_{ij}^{pp} = \lambda\frac{\partial g}{\partial \sigma_{ij}}, \tag{6}$$

where $d\varepsilon_{ij}^{pp}$ represents the plastic strain increment; g is the plastic potential function; λ is a non-negative scale factor which changes with the loading history.

Combing Eqs. (5) and (6), the expression of the relationship between plastic strains is

$$d\varepsilon_r^p = -N_\psi d\varepsilon_\theta^p \,. \tag{7}$$

2.7 Critical Supporting Pressure

When the internal support pressure P_i is lower than a critical value P_i^c, the plastic zone around the circular opening is formed. Therefore, before calculating the stress and deformation in the plastic zone of rock mass, it is first necessary to determine whether the rock mass will produce a plastic zone under a given supporting pressure. The critical condition of the plastic zone in rock mass is selected as the stress boundary condition to derive the critical supporting pressure. The critical condition for the plastic zone in rock mass is that the radius of plastic zone is equal to the tunnel radius. From this critical condition, the radial and tangential stresses at the tunnel face should meet the stress conditions as shown in follows:

$$\begin{cases} \sigma_r + 2\sigma_\theta = 3P_0 \\ f(\sigma_r,\sigma_\theta) = 0 \\ \sigma_r = P_i^c \,. \end{cases} \tag{8}$$

Combing the above boundary conditions, P_i^c can be calculated by using of the peak strength parameter and the initial stress for the M-C yield criterion rock mass:

$$P_{ic} = \frac{3P_0 - 2Y(P_{ic})}{2N(P_{ic})+1} \,. \tag{9}$$

3. Establishment of Mechanical Model

3.1 Approximate Assumption

The closed-form solutions are obtained using the linear M-C or non-linear H-B failure criterion for both elastic-perfectly plastic and elastic-brittle-plastic rock masses. Due to the nonlinear failure envelope for the strain-softening rock mass, developing a closed-form solution following the H-B criteria appears to be difficult. Furthermore, the changing confining stress of the plastic zone will make this work more difficult. In this condition, the finite difference approach introduced by Brown et al. (1983) is used to solve this problem. It is assumed that the plastic zone is divided into a set of concentric-annuluses using the same method and the thickness of each annulus is the same. Fig. 6 shows that $r_{(i)}$ and $r_{(i\text{-}1)}$ is the radius of the inner and outer boundaries of the ith annulus, respectively. Regarding the rock mass in the plastic zone, the radius of each annulus is normalized, as shown in Eq. (10), and the schematic diagram of rock mass stratification in the plastic zone is shown in Fig. 6.

$$\begin{cases} \rho_{(i-1)} = r_{(i-1)} / R_p \\ \rho_{(i)} = r_{(i)} / R_p \end{cases} \tag{10}$$

3.2 Stress and Deformation in the Plastic Zone

According to the normalization of radius, at the boundary of elastoplastic zone, that is, the rock mass stress at the boundary obeys the stress condition in the elastic zone and the stress condition in the plastic respectively, as shown in Eq. (11):

$$\begin{cases} \sigma_{r(1)} + 2\sigma_{\theta(1)} = 3P_0 \\ f(\sigma_{r(1)}, \sigma_{\theta(1)}) = 0. \end{cases} \tag{11}$$

Substituting the M-C yield criterion expression into Eq. (11), it can be transformed into

$$\begin{cases} 3P_0 - \left[2N\left(\sigma_{r(1)}\right)+1\right]\sigma_{r(1)} - 2Y\left(\sigma_{r(1)}\right) = 0 \\ \sigma_{\theta(1)} = 1.5P_0 - 0.5\sigma_{r(1)}. \end{cases} \tag{12}$$

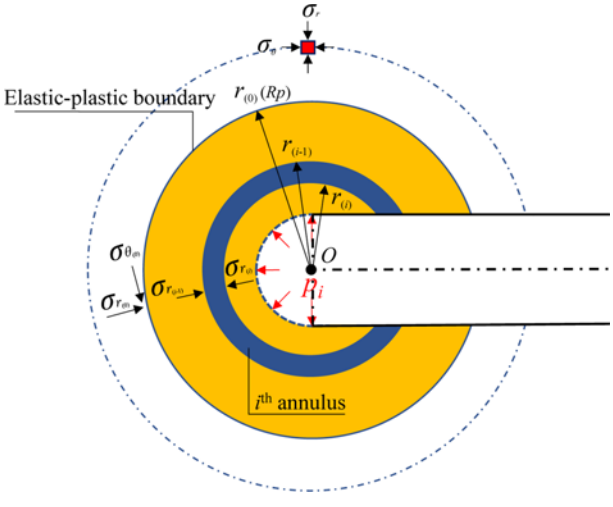

Fig. 6. Normalized Plastic Zone with the Finite Number of Annuli

Furthermore, the radial and tangential strains generated by elasticity at the elastoplastic boundary can be obtained using Hooke's law, as shown in Eq. (13):

$$\begin{cases} \varepsilon^e_{r(1)} = \dfrac{1}{E_{(\sigma_{r(1)})}}\left[(1+v)\sigma_{r(1)} - 3vP_0\right] \\ \varepsilon^e_{\theta(1)} = \dfrac{1}{2E_{(\sigma_{r(1)})}}\left[3(1-v)P_0 - (1+v)\sigma_{r(1)}\right], \end{cases} \tag{13}$$

where the radial and tangential strain superscript e represents the radial and tangential strain generated by elasticity.

Since a fixed step length increment is used to stratify the rock mass in plastic zone, the finite difference solution process of plastic zone also uses a fixed step difference method, which can be used to obtain the normalized radius iteration of any annulus, as shown in Eq. (14):

$$\Delta\rho = \rho_{(i)} - \rho_{(i-1)}. \tag{14}$$

At the same time, the radial and tangential stresses of the ith annulus in plastic zone obey the yield criterion. However, since the strength parameter is related to the radial stress, the value of strength parameter of each annulus is different, which is controlled by the radial stress ($\sigma_{r(i)}$). Therefore, the expression of yield criterion for any annulus is as follows:

$$f(\sigma_{r(i)}, \sigma_{\theta(i)})^{M-C} = \sigma_{\theta(i)} - \sigma_{r(i)} - F(\sigma_{r(i)}). \tag{15}$$

Combining any annulus rock mass to satisfy the equilibrium equation, its expression is shown in Eq. (16):

$$\frac{d\sigma_{r(i)}}{d\rho_{(i)}} + \frac{2\left(\sigma_{r(i)} - \sigma_{\theta(i)}\right)}{\rho_{(i)}} = 0. \tag{16}$$

Combining Eq. (15), Eq. (16) can be reformulated as

$$\frac{d\sigma_{r(i)}}{d\rho_{(i)}} = -\frac{2\left(\sigma_{r(i)} - \sigma_{\theta(i)}\right)}{\rho_{(i)}} = \frac{2\left(\sigma_{\theta(i)} - \sigma_{r(i)}\right)}{\rho_{(i)}} = \frac{2F(\sigma_{r(i)})}{\rho_{(i)}}. \tag{17}$$

The third-order Runge-Kutta method is used to solve the radial stress expression of the ith annulus, as shown in Eq. (18):

$$\sigma_{r(i)} = \sigma_{r(i\text{-}1)} + \frac{1}{6}\left(k_1 + 4k_2 + k_3\right), \tag{18}$$

where

$$k_1 = \frac{2\Delta\rho F\left(\sigma_{r(i\text{-}1)}\right)}{\rho_{(i-1)}},$$

$$k_2 = \frac{2\Delta\rho F\left(\sigma_{r(i\text{-}1)} + \dfrac{k_1}{2}\right)}{\rho_{(i-1)} + 0.5\Delta\rho},$$

$$k_3 = \frac{2\Delta\rho F\left(\sigma_{r(i\text{-}1)} - k_1 + 2k_2\right)}{\rho_{(i-1)} + \Delta\rho}.$$

Furthermore, according to Eq. (15), the tangential stress expression of the ith annulus can be obtained, as shown in Eq. (19):

$$\sigma_{\theta(i)} = \sigma_{r(i)} + F\left(\sigma_{r(i)}\right). \tag{19}$$

Based on the plastic increment theory, the strain of rock mass in the plastic zone is solved, which be divided into elastic strain and plastic strain:

$$\begin{Bmatrix} \varepsilon_r \\ \varepsilon_\theta \end{Bmatrix} = \begin{Bmatrix} \varepsilon_r^e \\ \varepsilon_\theta^e \end{Bmatrix} + \begin{Bmatrix} \varepsilon_r^p \\ \varepsilon_\theta^p \end{Bmatrix}. \tag{20}$$

According to Hooke's law, the expression of elastic strain in the plastic zone can be obtained:

$$\begin{Bmatrix} \varepsilon_{r(i)}^e \\ \varepsilon_{\theta(i)}^e \end{Bmatrix} = \frac{1}{E_{(i)}} \begin{bmatrix} 1 & -2v \\ -v & 1-v \end{bmatrix} \begin{Bmatrix} \sigma_{r(i)} \\ \sigma_{\theta(i)} \end{Bmatrix}. \tag{21}$$

The displacement compatibility equation is shown as follows:

$$\begin{cases} \dfrac{d\varepsilon_\theta}{d\rho} + \dfrac{\varepsilon_\theta - \varepsilon_r}{\rho} = 0 \\ \varepsilon_r = \dfrac{du}{dr} \\ \varepsilon_\theta = \dfrac{u}{r}. \end{cases} \tag{22}$$

Combining Eq. (20), Eq. (22) can be reformulated as

$$\frac{d\varepsilon_\theta^p}{d\rho} = -\frac{\left(\varepsilon_\theta^p - \varepsilon_r^p\right) + \left(\varepsilon_\theta^e - \varepsilon_r^e\right)}{\rho} - \frac{d\varepsilon_\theta^e}{d\rho}. \tag{23}$$

Equation (24) can be obtained by the non-associative flow rule,

$$\frac{d\varepsilon_r^p}{d\rho} = -N_\phi \frac{d\varepsilon_\theta^p}{d\rho}. \tag{24}$$

The elastic and plastic tangential strain increments are as follows:

$$\begin{cases} \Delta\varepsilon_\theta^e = -\left(\varepsilon_{\theta(i-1)}^e - \varepsilon_{\theta(i)}^e\right) \\ \Delta\varepsilon_\theta^p = -\left(\varepsilon_{\theta(i-1)}^p - \varepsilon_{\theta(i)}^p\right). \end{cases} \tag{25}$$

Combining Eqs. (23), (24) and (25), the forward Euler method is used to solve the expressions of plastic tangential strain and radial strain of the ith annulus, shown as follows:

$$\begin{cases} \varepsilon_{\theta(i)}^p = \varepsilon_{\theta(i-1)}^p + \dfrac{-\left(\varepsilon_{\theta(i-1)}^e - \varepsilon_{r(i-1)}^e\right) + \left(\varepsilon_{\theta(i-1)}^p - \varepsilon_{r(i-1)}^p\right)}{\rho_{(i-1)}} \Delta\rho - \dfrac{\Delta\varepsilon_\theta^e}{\Delta\rho} \\ \varepsilon_{r(i)}^p = \varepsilon_{r(i-1)}^p + \Delta\rho\left(-N_\phi \dfrac{\Delta\varepsilon_\theta^p}{\Delta\rho}\right). \end{cases} \tag{26}$$

Therefore, the expression of total strain in the plastic zone of the ith annulus is as follows:

$$\begin{Bmatrix} \varepsilon_{r(i)} \\ \varepsilon_{\theta(i)} \end{Bmatrix} = \begin{Bmatrix} \varepsilon_{r(i)}^e \\ \varepsilon_{\theta(i)}^e \end{Bmatrix} + \begin{Bmatrix} \varepsilon_{r(i)}^p \\ \varepsilon_{\theta(i)}^p \end{Bmatrix}. \tag{27}$$

If the finite difference step length ($\Delta\rho$) is small enough, according to the mechanical parameter model, the mechanical parameters of rock mass in the (i+1)th annulus can be replaced by the mechanical parameters of rock mass under the radial stress condition of the ith annulus, so as to perform the next annulus calculation.

The finite difference iterative convergence stop condition is: when the radial stress of the nth annulus is equal to the supporting pressure P_i of the tunnel face, the iterative calculation process stops. The iterative stop discriminant expression, as shown in Eq. (28):

$$\sigma_{r(n)} = P_i. \tag{28}$$

At this time, R_p can be obtained from the ρ_n expression:

$$R_p = \frac{R}{\rho_{(n)}}. \tag{29}$$

And the displacement around the tunnel can be obtained from Eqs. (22) and (27), and the expressions are shown as follows:

$$u_{(n)} = \varepsilon_{\theta(n)} \cdot R. \tag{30}$$

3.3 Stress and Deformation in the Elastic Zone

The boundary conditions of the internal and external interface stress of the elastic zone can be expressed as

$$\begin{cases} (\sigma_r)_\infty = P_0 \ ; \ (\sigma_\theta)_\infty = P_0 \\ (\sigma_r)_e = \sigma_r^{R_p} \ ; \ (\sigma_\theta)_e = \sigma_\theta^{R_p}. \end{cases} \tag{31}$$

According to the stress continuity condition, the radial and tangential stresses at the inner boundary are equal to the radial and tangential stresses at the outer boundary of the plastic zone, i.e.,

$$\begin{cases} \sigma_r^{R_p} = \sigma_{r(1)} \\ \sigma_\theta^{R_p} = \sigma_{\theta(1)}. \end{cases} \tag{32}$$

Using the elastic theory under the condition of spherical symmetry, the stress and displacement in the elastic zone can be obtained, shown as follows:

$$\begin{cases} \sigma_\theta^e = P_0 + \dfrac{1}{2}(P_0 - \sigma_{r(1)}) \dfrac{R_p^3}{r^3} \\ \sigma_r^e = P_0 - (P_0 - \sigma_{r(1)}) \dfrac{R_p^3}{r^3} \\ u_e = \dfrac{1+v}{2E_{(\sigma_{r(1)})}} \left(p_0 - \sigma_{r(1)}\right) \dfrac{R_p^3}{r^2}. \end{cases} \tag{33}$$

The expression of strain component in the elastic zone is shown in Eq. (24):

$$\begin{Bmatrix} \varepsilon_{r,e}^e \\ \varepsilon_{\theta,e}^e \end{Bmatrix} = \frac{1}{E_{(\sigma_{r(1)})}} \begin{bmatrix} 1 & -2v \\ -v & 1-v \end{bmatrix} \begin{Bmatrix} \sigma_{r(1)} \\ \sigma_{\theta(1)} \end{Bmatrix}. \tag{34}$$

3.4 Solution Process

Based on the previous derivation of mechanical expressions for the plastic zone and elastic zone of rock mass, the calculation steps are summarized as follows:

1. Calculate p_{ic} using Eq. (9). If $P_i \geq P_i^c$, no plastic zone is formed, thus elastic solution should be used for the whole region. Then the stress and displacement of the elastic zone are solved using Eq. (33). But the boundary conditions at this time will become P_0. Otherwise, the plastic zone and elastic zone exist.
2. Input the expression of rock mass mechanical parameters changing with confining stress, initial stress P_0, and tunnel radius R. At the same time, it is necessary to determine the iteration step length of the calculation.
3. Calculate $\sigma_{r(1)}$ and $\sigma_{\theta(1)}$ by Eq. (11), and calculate $\varepsilon^e_{r(1)}$ and $\varepsilon^e_{\theta(1)}$ by Eq. (13).
4. Calculate $\sigma_{r(i)}$ and $\sigma_{\theta(i)}$ by Eqs. (18) and (19), respectively.
5. Calculate $\varepsilon_{r(i)}$ and $\varepsilon_{\theta(i)}$ by Eq. (27).
6. When $\sigma_{r(n)} = P_i$, stop the calculation loop and calculate the plastic radius R_p and face extrusion deformation $u_{(n)}$ by Eqs. (29) and (30), respectively. Otherwise, repeat step 4) – 6) and set $i = i + 1$.

4. Plausibility Verification

4.1 Accuracy Analysis of Proposed Model

To investigate how the results are influenced by the magnitude of $\Delta\rho$ in Eq. (17), i.e., the number of annuli n, 12 values of n are considered in this paper, i.e., 10, 50, 100, 200, 300, 400, 500, 600, 700, 800, 900 and 1000. It can be seen that with the continuous increase of the number of annuli, the calculation results gradually tend to be stable as shown in Fig. 7. The radius of the plastic zone tends to be stable when the number of annuli reaches 100, and the extrusion deformation of the tunnel face tends to be stable when the number of annuli reaches 300. Therefore, when using the proposed model to analyze the stress and deformation of the tunnel face, the number of iteration annuli must be at least 300 to ensure the accuracy of the calculation results.

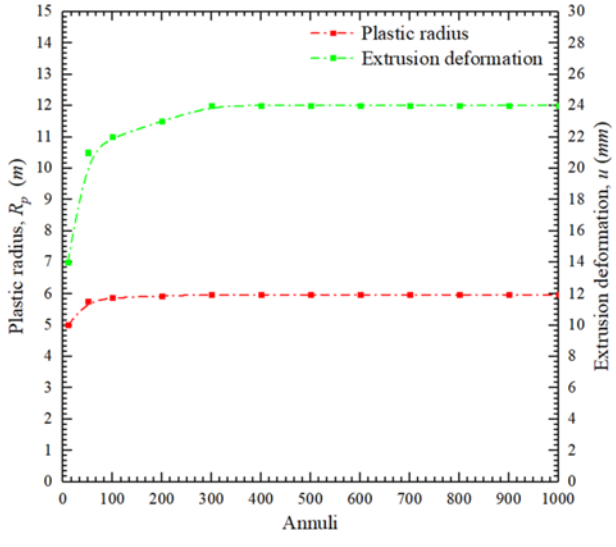

Fig. 7. Variation Curve of Plastic Radius and Extrusion Deformation Value of Tunnel Face with the Number of the Annulus

4.2 Verification Example

In order to verify the accuracy of the theoretical derivation, the calculation results based on this paper will be compared with the existing research results.

Based on the M-C strength criterion, Pierpaolo Oreste (Oreste, 2013) derives an analytical solution for the extrusion deformation of tunnel face considering the elastic-brittle-plastic characteristics of rock mass, as shown in Eq. (36), but it does not consider the strain-softening characteristics of rock mass.

Plastic zone radius:

$$\frac{R_p}{R} = \left[\frac{\left(\frac{1.5p_0 - f_{penk}}{N_{peak} + 0.5} + \frac{f_{res}}{N_{res} - 1} \right)}{\left(p + \frac{f_{res}}{N_{res} - 1} \right)} \right]^{\frac{1}{2(N_{res} - 1)}}, \tag{35}$$

where

$$f_{peak} = \frac{2c_{peak}\cos\varphi_{peak}}{1 - \sin\varphi_{peak}};\ N_{peak} = \frac{1 + \sin\varphi_{peak}}{1 - \sin\varphi_{peak}};$$

$$f_{res} = \frac{2c_{res}\cos\varphi_{res}}{1 - \sin\varphi_{res}};\ N_{res} = \frac{1 + \sin\varphi_{res}}{1 - \sin\varphi_{res}}.$$

The face extrusion deformation:

$$u = \frac{n}{k+1} r - \frac{l}{k+m+1} r^{m+1} + \left[u_{R_p} R_p^k - \frac{n}{k+1} R_p^{k+1} + \frac{l}{k+m+1} R_p^{m+k+1} \right] r^{-k}, \tag{36}$$

where

$$n = \frac{f_{res}}{E}\left[(k - kv - 2v) - \frac{1 - kv + N_{res}(k - kv - 2v)}{N_{res} - 1} \right] + \frac{p_0}{E}(2kv - k + 2v - 1),$$

$$l = -\frac{p + \left(\frac{f_{res}}{N_{res} - 1} \right)}{E} \frac{1}{R^m} \left[1 - kv + N_{res}(k - kv - 2v) \right],$$

$$m = 2\left(N_{res} - 1 \right),$$

$$u_{R_p} = \frac{1 + v}{2E}\left(p_0 - \sigma_{r,R_p} \right) R_p,$$

$$\sigma_{r,R_p} = \frac{1.5p_0 - f_{peak}}{N_{peak} + 0.5},$$

where and c_{res} and φ_{res} are the residual cohesion and friction angle of rock mass, respectively; c_{peak} and φ_{peak} are the peak cohesion

Table 2. Summary of the Numerical Parametric Analysis

Symbol	Variables
P_0 (MPa)	2, 2.5, 3, 3.5, 4, 4.5, 5
c_p (MPa)	0.2
c_r (MPa)	0.2
φ_p(°)	30
φ_r(°)	30
E (GPa)	0.4
ψ(°)	5
γ (kN/m^3)	20
μ	0.3
R (m)	3

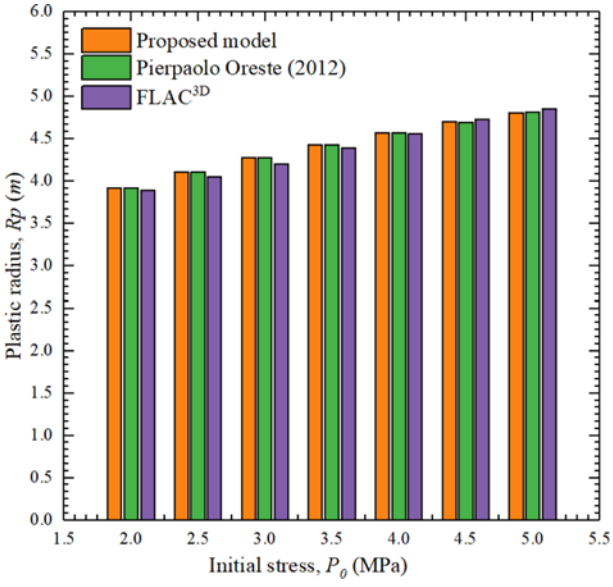

Fig. 8. Comparison and Verification of Plastic Zone Radius

and friction angle of rock mass, respectively; E and v are the Young's modulus and the Poisson ratio of rock mass; and ψ is the dilatancy angle.

If the residual strength is equal to the peak strength, it can be degenerated into an elastic-perfectly plastic model. In addition, the rock mass mechanical parameter confining stress model in the proposed model is set as the mechanical parameter unchanged, that is, the mechanical parameter change characteristics under the variable confining stress condition are not considered. At this time, the proposed model degenerates into an elastic-perfectly plastic model. To validate the accuracy and applicability of the model established in this work, the results obtained by the proposed model, numerical model and Pierpaolo Oreste models are compared in this section.

In order to ensure the accuracy of the finite difference calculation, according to the analysis result of the Section 4.1, the fixed difference step size ($\Delta\rho$) is set to 10^{-3}, and the calculation parameters is shown in Table 2.

It can be seen from the calculation results in Figs. 8 and 9 that the radius of plastic zone obtained by the proposed model is

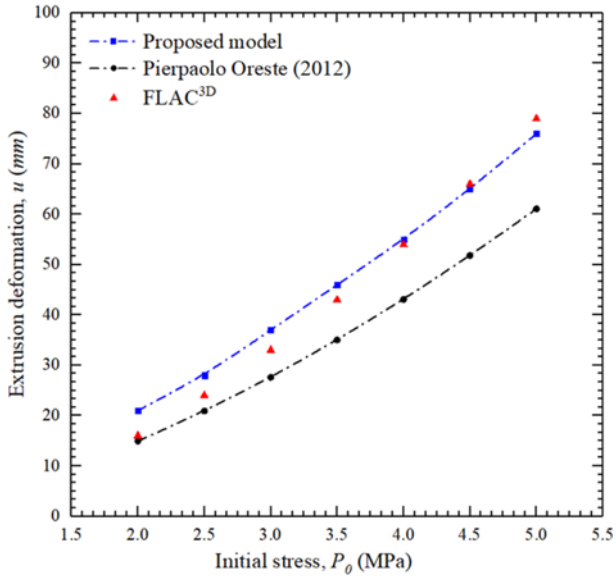

Fig. 9. Comparison and Verification of Extrusion Deformation of the Tunnel Face

highly consistent with the results obtained by the Pierpaolo Oreste model and the numerical model. Among them, the extrusion deformation error of the tunnel face is relatively large. The reason is that the mathematical approximate solution method is used in the process of deriving the extrusion deformation of tunnel face, which leads to errors with the closed-form solution, but the overall error is within an acceptable range. Therefore, it can be seen from the above comparative analysis results that the calculation method for the extrusion deformation and plastic zone of tunnel face using the finite difference method is more reasonable and accurate.

5. Discussion and Analysis

5.1 The Necessity of considering Changes of Mechanical Parameters

In this part, both the Pierpaolo Oreste model and the proposed model are utilized to conduct certain parametric calculations in order to determine whether the effect of confining stress needs to be considered in the calculation process. The calculation parameters of analysis conditions are listed in Table 3.

By comparing the results calculated by the Pierpaolo Oreste model and the proposed model, it can be seen from Fig. 11 that the difference between the plastic radius when the changes in the mechanical parameters of rock mass are considered and the plastic radius when the changes in the mechanical parameters of rock mass are not considered is small when the initial stress is small. However, with the increase of the initial stress, the difference between the plastic radius obtained by the two calculation methods gradually increases. Moreover, the plastic radius obtained when considering the change of the mechanical parameters of rock mass is larger than that of the plastic radius without considering the change of the mechanical parameters of the rock mass, which

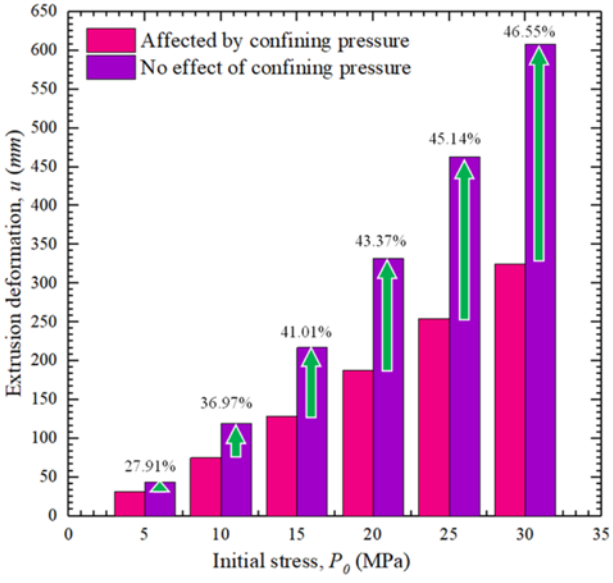

Fig. 10. Extrusion Deformation

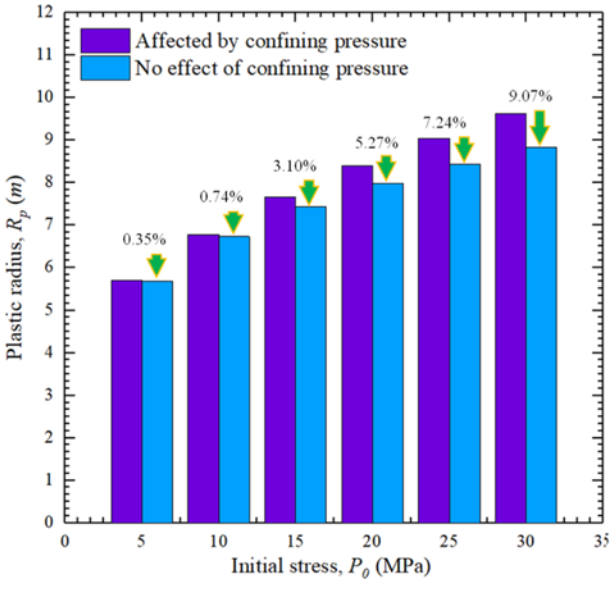

Fig. 11. Plastic Radius

is mainly caused by the shear strength characteristics of rock mass. If the changes in the mechanical parameters of rock mass are not considered, it is actually considered that the shear yield surface of the rock mass increases proportionally with the confining stress, thereby increasing the shear strength of the rock mass. The shear strength of rock mass under high confining stress presents significant non-linear characteristics, and its shear strength increase rate gradually decreases with the increase of confining stress. As a result, the plastic radius obtained when considering the change of mechanical parameters is larger than the result that the change of rock mass parameters is not considered. If the shear strength parameters of rock mass are not considered, the plastic radius will be smaller than the actual radius of rock mass, and with the increase of the initial stress, the difference in the radius of the plastic zone will gradually increase. This also illustrates the importance of considering the changes in mechanical parameters of rock mass when calculating the plastic zone in front of the tunnel face in high initial stress soft rock.

As shown in Fig. 10, when the initial stress is small, the difference of face extrusion deformation between the two calculation methods considering and not considering the changes in mechanical parameters of the rock mass is small. However, with the increase of the initial stress, the extrusion deformation obtained without considering the change of rock mass parameters is obviously greater than that obtained when considering the change of rock mass parameters. And with the increase of the initial stress, the difference in the extrusion deformation obtained by the two calculation methods shows an increasing trend, which is caused by the characteristics of rock mass deformation parameters. When calculating the extrusion deformation without considering the change of the rock mass parameters, the influence of the confining stress on the Young's modulus of rock mass is actually ignored. Therefore, the stiffness of rock mass under confining stress is underestimated, resulting in that the extrusion deformation is significantly greater than the result of the extrusion deformation considering the changes in the mechanical parameters of rock mass. It can be seen that if the deformation parameters of rock mass are not considered, the calculated extrusion deformation will be significantly greater than the actual extrusion deformation value, and with the increase of the initial stress, the calculation error of the extrusion deformation shows an increasing trend.

The rock mass parameter mechanical model of variable confining stress used in this analysis is not the only form, and different soft rock types may induce different variable confining stress parameter models. In the actual engineering application, the corresponding variable confining stress parameter change model can be obtained according to the experiment and brought into the proposed model for analysis.

5.2 Effect of the Supporting Pressure

Figure 12 presents the results of the face extrusion deformation

Table 3. Calculation Parameters

Fixed parameter	Calculation parameters	
R = 3 m; P_0 = 5 MPa, 10 MPa, 15 MPa, 20 MPa, 25 MPa, 30 MPa; $\psi = 0$; $\mu = 0.3$	The parameters considering the confining stress	The parameters without considering the confining stress (the confining stress is 0)
	$E = 0.9(\sigma_3 + 1)^{0.82}$	0.9
	$\varphi = -4.13 ln(\sigma_3 + 1) + 30$	30
	$c = 0.1(\sigma_3 + 1)^{0.53}$	0.1

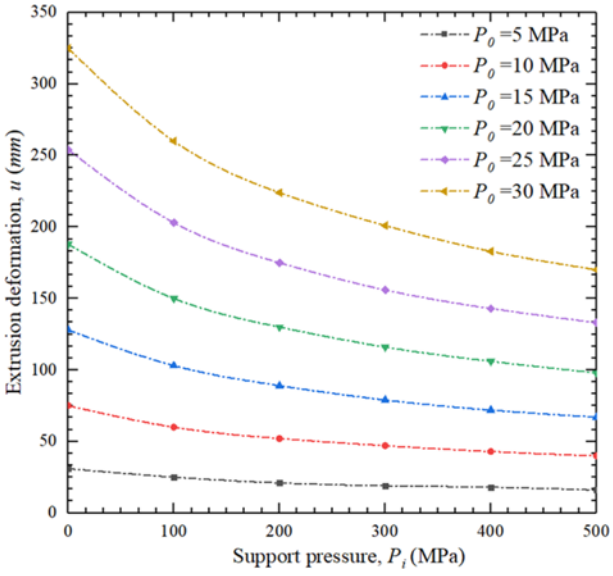

Fig. 12. Change Curve of Extrusion Deformation with Support Pressure

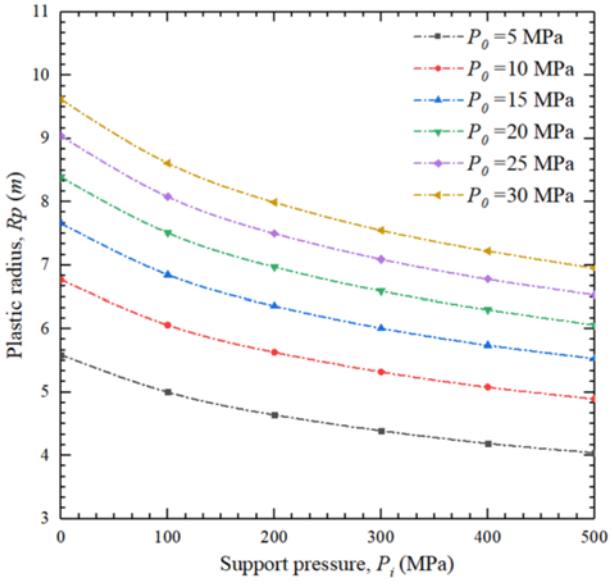

Fig. 13. Change Curve of the Plastic Radius with Support Pressure

under different support pressure and initial stress. It can be seen that the face extrusion deformation decreases with increasing support pressure when the initial stress is constant. But the reduction value of face extrusion deformation increases with increasing the initial stress. For instance, when the initial stress is 5 MPa, 10 MPa, 15 MPa, 20 MPa, 25 MPa, and 30 MPa, the support pressure increases from 0 to 100 kPa, the reduction values are 6 mm, 15 mm, 25 mm, 38 mm, 51 mm, and 65 mm, respectively. Fig. 13 presents the results of the plastic radius under different support pressure and initial stress. It can be seen that the plastic radius decreases with increasing support pressure when the initial stress is constant, but the reduction value of plastic radius increases with increasing the initial stress. For instance, when the initial stress is 5 MPa, 10 MPa, 15 MPa, 20 MPa, 25 MPa, and 30 MPa, the support pressure increases from 0 to 100 kPa, the reduction values are 0.59 m, 0.71 m, 0.81 m, 0.88 m, 0.96 m, and 1.01 m, respectively. From this analysis, it can be seen that under the conditions of high initial stress, the effective provision of support pressure is of great significance for controlling the stability of the tunnel face and ensuring the safety of tunnel.

When the strength properties of rock mass do not guarantee the stability of its face, fibreglass reinforcements are generally added. Because they confine the tunnel face by applying of concentrated pressures which are balanced by other forces that develop lower down in the anchoring zone. Because of the brittleness of the fibreglass materials, they are easily cut by excavating machinery. As a result, this reinforcing approach type does not affect excavation efficiency. Several researchers have explored the topic of excavation face stability in deep tunnels with fiberglass reinforcements in recent years (Eberhardt, 2001; Yoo, 2002; Yoo and Shin, 2003). All of these efforts have enabled to investigate the role and action mechanisms of fiberglass reinforcements on tunnel face stability.

5.3 Discussion on the Applicability of the Proposed Model for a Horseshoe Tunnel Face

The proposed model is based on circular tunnel section, thus there are certain limitations when using this method for non-circular caverns. Therefore, the analysis of non-circular caverns is carried out in this section. At present, the commonly used processing method is to convert non-circular cross-sections into proxy circular cross-sections according to a certain equivalent method. In principle, the equivalent method can be roughly divided into mechanical equivalent method and area equivalent method. For a horseshoe-shaped section with height and span respectively h and b (as shown in Fig. 14(a)), the equivalent circle radius R is taken as a quarter of the sum of height h and span b (Eq. (37)). The other three calculation methods are shown in Eqs. (38), (39), and (40), corresponding to the three types of tunnel cross-sections in Figs. 14(b), 14(c), and 14(d):

$$R = (h+b)/4\,, \tag{37}$$

$$R = \sqrt{h^2 + (b/2)^2}\ /\ 2\cos[(2h/b)]\,, \tag{38}$$

$$R = b/2\sin(a/2)\,, \tag{39}$$

$$R = (a_1 + a_2)/2\,. \tag{40}$$

Since the calculation result of Eq. (2) has greater adaptability and accuracy, it is adopted in the calculation of this work. The extrusion deformation and plastic radius of the horseshoe shape tunnel face are calculated using FLAC^{3D} numerical calculation software. Because the FLAC^{3D} cannot realize the change of the rock mass mechanical parameters with the confining stress, in order to compare with the numerical calculation results, the variable confining stress calculation model is degenerated into a constant confining stress calculation model. In order to analyze the rationality of the proposed model in this work used in non-circular caverns, 8 analysis conditions are set up. The numerical calculation model

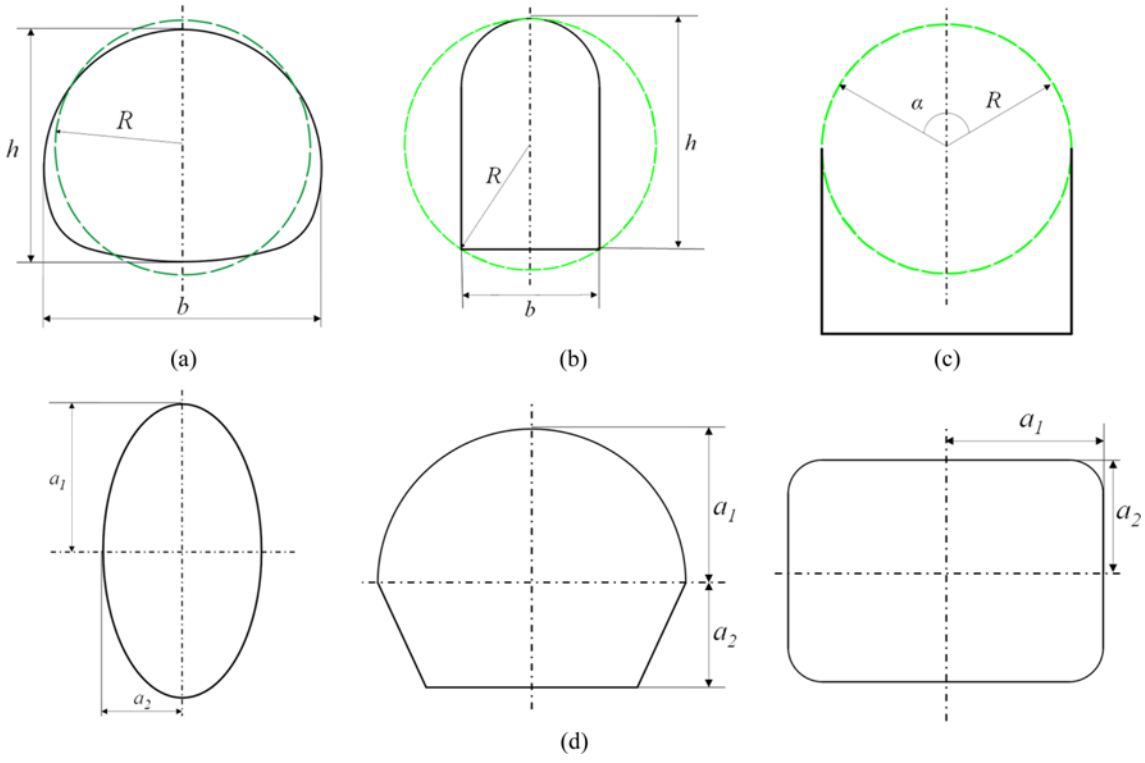

Fig. 14. Simplified Calculation of Equivalent Circle Radius: (a) Method of Equivalent Circle Radius, (b) Method of Circumscribed Circle Radius, (c) Method of Arch Radius, (d) Half of Sum of Maximum and Minimum Radii

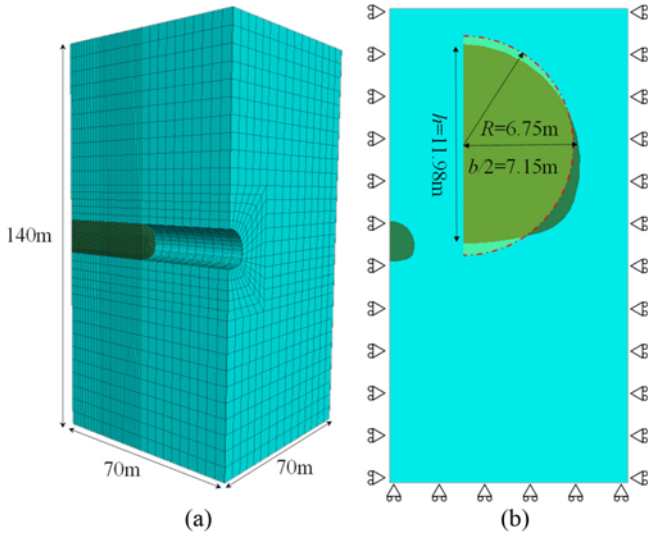

Fig. 15. Numerical Calculation Model: (a) Computational Domain and Boundary Conditions, (b) Front View of Calculation Model

and calculation parameters are shown in Table 3 and Fig. 15, respectively.

It can be seen from the calculation results of face extrusion deformation that the calculated value of the equivalent circle radius is similar to that the numerical model, and the error between the two calculation results is small (as shown in Fig. 16), i.e., the maximum error is 12%, the minimum error is 2.13%, and the average is 7.03%. Similarly, the calculation results of the plastic radius of the two models are relatively similar (as shown in Fig. 17), i.e., the maximum error is 10.40%, the minimum error is 0.23%, and the average error is 4.13%. It can be seen that the proposed model has a better application effect on non-circular caverns (horseshoe shape tunnels), and the calculation results are more accurate.

6. Conclusions

Based on the relationship between the rock mechanical parameters and confining stress, the elastic-plastic solution for stress and deformation states around tunnel face was proposed which considers the influence of confining stress on the rock mechanical parameters. And the rationality of the proposed model was verified through the comparative analysis with the numerical model and another theoretical model (Pierpaolo Oreste's model). The main conclusions are summarized as follows:

1. The relationship between rock mechanical parameters and confining pressure was analyzed through the some existing rock triaxial test data, i.e., the Young's modulus, the internal friction angle, and the cohesive show a nonlinear increasing trend with the increase of confining stress; however, Poisson's ratio has no significant change trend with the increase of confining stress. And a new model considering the influence of confining stress is proposed on the basis of M-C failure critical and the non-associated flow rule. Then the rationality

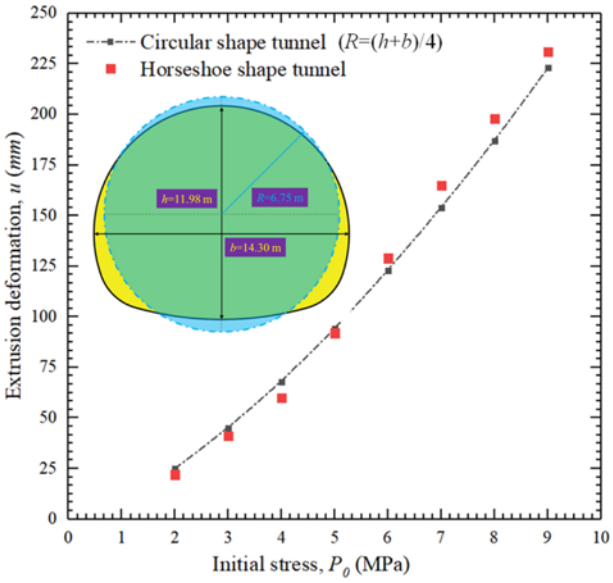

Fig. 16. Change Curve of Extrusion Deformation with Initial Stress (horseshoe shape tunnel)

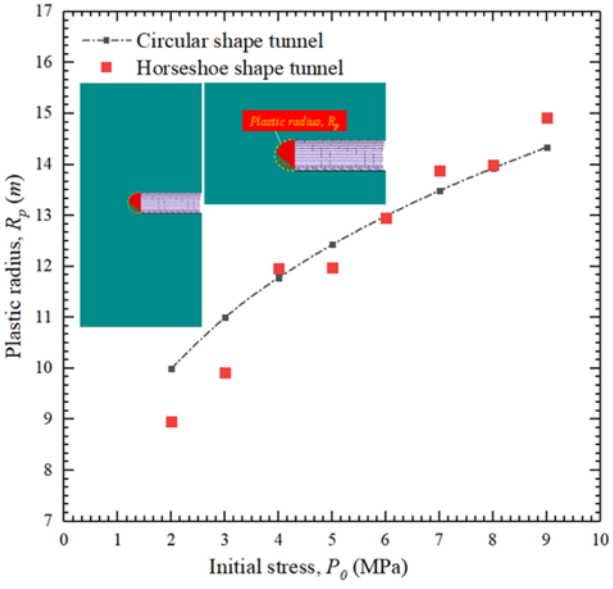

Fig. 17. Change Curve of the Plastic Radius with Initial Stress (horseshoe shape tunnel)

of the proposed model is verified through the comparative analysis with the numerical model and another theoretical model (Pierpaolo Oreste's model).

2. A comparative analysis of the variable confining stress model and constant confining stress model is carried out through calculation examples, and the results show that: regardless of the influence of confining stress on the mechanical parameters of rock mass, the plastic radius of the tunnel face will be smaller than the actual value, and the face extrusion deformation value will be larger. It is emphasized that the influence of confining stress on the mechanical parameters of rock mass should be considered in actual engineering calculations, especially under the conditions of high initial stress.
3. The face extrusion deformation and plastic radius gradually decrease with the increase of the face support pressure of tunnel. Similarly, this effect is more pronounced under the conditions of high initial stress. Therefore, in actual engineering, especially in the squeezing tunnels, the reasonable design of the fibreglass bolts is of great significance to ensure the stability of the tunnel face and the safe advancement of the tunnel.
4. Combined with the numerical calculation software, the error of face extrusion deformation and plastic radius between the two calculation results is small, i.e., the average error of extrusion deformation is 7.03% and the average error of plastic radius is 4.13%. It can be seen that the proposed model in this paper has a better application effect on non-circular caverns (horseshoe shape tunnels), and the calculation results are more accurate.

Acknowledgments

This work was supported by the Project of China Railway Science and Technology Research and Development Plan(Grant Nos. P2019G038).

ORCID

Not Applicable

References

Alejano LR, Alonso E, Rodríguez-Dono A, Fernández-Manín G (2010) Application of the convergence-confinement method to tunnels in rock masses exhibiting Hoek–Brown strain-softening behaviour. *International Journal of Rock Mechanics and Mining Sciences* 47(1):150-160, DOI: 10.1016/j.ijrmms.2009.07.008

Alejano LR, Rodríguez-Dono A, Veiga M (2012) Plastic radii and longitudinal deformation profiles of tunnels excavated in strain-softening rock masses. *Tunnelling and Underground Space Technology* 30:169-182, DOI: 10.1016/j.tust.2012.02.017

Alonso E, Alejano LR, Varas F, Fdez-Manin G, Carranza-Torres C (2010) Ground response curves for rock masses exhibiting strain-softening behaviour. *International Journal for Numerical & Analytical Methods in Geomechanics* 27(13):1153-1185, DOI: 10.1002/nag.315

Barla G (2016) Full-face excavation of large tunnels in difficult conditions. *Journal of Rock Mechanics & Geotechnical Engineering* 3(1):294-303, DOI: 10.1016/j.jrmge.2015.12.003

Brown ET, Bray JW, Ladanyi B, Hoek E (1983) Ground response curves for rock tunnels. *Journal of Geotechnical Engineering* 109(1):15-39, DOI: 10.1061/(ASCE)0733-9410(1983)109:1(15)

Cai M, Kaiser PK, Tasaka Y, Minami M (2007) Determination of residual strength parameters of jointed rock masses using the GSI system. *International Journal of Rock Mechanics & Mining Sciences* 44(2): 247-265, DOI: 10.1016/j.ijrmms.2006.07.005

Cantieni L, Anagnostou G, Hug R (2011) Interpretation of core extrusion measurements when tunnelling through squeezing ground. *Rock Mechanics & Rock Engineering* 44(6):641-670, DOI: 10.1007/

s00603-011-0170-5

Carranza-Torres C, Fairhurst C (1999) The elasto-plastic response of underground excavations in rock masses that satisfy the Hoek–Brown failure criterion. *International Journal of Rock Mechanics & Mining Sciences* 36(6):777-809, DOI: 10.1016/S0148-9062(99)00047-9

Carranza-Torres C, Fairhurst C (2000) Application of the convergence-confinement method of tunnel design to rock masses that satisfy the Hoek-Brown failure criterion. *Tunnelling and Underground Space Technology* 15(2): 187-213, DOI: 10.1016/S0886-7798(00)00046-8

Cheng HT (2020) Solution of a bolted spherical cavity in elastoplastic medium and its application to extrusion analysis of tunnel face. *Rock Mechanics and Rock Engineering* 53(6):85-93, DOI: 10.1007/s00603-020-02086-3

Cui L, Zheng JJ, Zhang RJ, Dong YK (2015) Elasto-plastic analysis of a circular opening in rock mass with confining stress-dependent strain-softening behaviour. *Tunnelling and Underground Space Technology* 50:94-108, DOI: 10.1016/j.tust.2015.07.001

Eberhardt E (2001) Numerical modelling of three-dimension stress rotation ahead of an advancing tunnel face. *International Journal of Rock Mechanics and Mining Ences* 38(4):499-518, DOI: 10.1016/S1365-1609(01)00017-X

Gholami R, Rasouli V (2014) Mechanical and elastic properties of transversely isotropic slate. *Rock Mechanics and Rock Engineering* 47(5):1763-1773, DOI: 10.1007/s00603-013-0488-2

Kim P (2006) Analytical solution for a circular opening in an elastic–brittle–plastic rock. *International Journal of Rock Mechanics and Mining Sciences* 43(4):616-622, DOI: 10.1016/j.ijrmms.2005.11.004

Lee YK, Pietruszczak S (2008) A new numerical procedure for elasto-plastic analysis of a circular opening excavated in a strain-softening rock mass. *Tunnelling and Underground Space Technology* 23(5): 588-599, DOI: 10.1016/j.tust.2007.11.002

Lunardi P (2008) Design and construction of tunnels: Analysis of controlled deformation in rocks and soils (ADECO-RS). Springer-Verlag, Heidelberg, Berlin, Germany, 30-45

Oreste P (2013) Face stabilization of deep tunnels using longitudinal fibreglass dowels. *International Journal of Rock Mechanics & Mining Sciences* 58(1):127-140, DOI: 10.1016/j.ijrmms.2012.07.011

Park KH, Tontavanich B, Lee JG (2008) A simple procedure for ground response curve of circular tunnel in elastic-strain softening rock masses. *Tunnelling and Underground Space Technology* 23(2):151-159, DOI: 10.1016/j.tust.2007.03.002

Serrano A, Olalla C, Reig I (2011) Convergence of circular tunnels in elastoplastic rock masses with non-linear failure criteria and non-associated flow laws. *International Journal of Rock Mechanics and Mining Sciences* 48(6):878-887, DOI: 10.1016/j.ijrmms.2011.06.008

Sharan SK (2003) Elastic-brittle-plastic analysis of circular openings in Hoek-Brown media. *International Journal of Rock Mechanics & Mining Sciences* 40(6):236-258, DOI: 10.1016/S1365-1609(03) 00040-6

Sharan SK (2005) Exact and approximate solutions for displacements around circular openings in elastic–brittle–plastic Hoek–Brown rock. *International Journal of Rock Mechanics & Mining Sciences* 42(4):542-549, DOI: 10.1016/j.ijrmms.2005.03.019

Sharan SK (2008) Analytical solutions for stresses and displacements around a circular opening in a generalized Hoek–Brown rock. *International Journal of Rock Mechanics & Mining Sciences* 45(1): 78-85, DOI: 10.1016/j.ijrmms.2007.03.002

Varas F, Alonso E, Alejano LR, Fdez.-Manin G (2005) Study of bifurcation in the problem of unloading a circular excavation in a strain-softening material. *Tunnelling and Underground Space Technology* 20(4):311-322, DOI: 10.1016/j.tust.2004.12.003

Vrakas A, Anagnostou G (2014) A finite strain closed-form solution for the elastoplastic ground response curve in tunnelling. *International Journal for Numerical and Analytical Methods in Geomechanics* 38(11):1131-1148, DOI: 10.1002/nag.2250

Wang S, Hong Z, Li C, Ge X (2011) A finite element implementation of strain-softening rock mass. *International Journal of Rock Mechanics & Mining Sciences* 48(1):67-76, DOI: 10.1016/j.ijrmms.2010.11.001

Wang SL, Yin XT, Tang H, Ge X (2010) A new approach for analyzing circular tunnel in strain-softening rock masses. *International Journal of Rock Mechanics & Mining Sciences* 47(1):170-178, DOI: 10.1016/j.ijrmms.2009.02.011

Yoo C (2002) Finite-element analysis of tunnel face reinforced by longitudinal pipes. *Computers & Geotechnics* 29(1):73-94, DOI: 10.1016/S0266-352X(01)00020-9

Yoo C, Shin HK (2003) Deformation behaviour of tunnel face reinforced with longitudinal pipes—laboratory and numerical investigation. *Tunnelling and Underground Space Technology* 18(4):303-319, DOI: 10.1016/s0886-7798(02)00101-3

Yu HS (2000) Cavity expansion methods in geomechanics. Springer Science+Business Media, Berlin, Germany, 192-199